






Extensive Analysis and Projection of the Impact of High-Risk Immunity Using a Mathematical Model That Incorporates a Convex Incidence Rate of Multiple Covid-19 Exposures

Mutairu Kayode Kolawole^{1*} , Morufu Oyedunsi Olayiwola¹ , Adedapo Ismaila Alaje¹ 

Abidoeye Kazeem Odeyemi¹ 

¹ Department of Mathematics, College of Science Engineering and Technology, Osogbo, Nigeria

Keywords

COVID-19,
Incidence rate,
High risk immunity,
Homotopy
perturbation method.

Abstract

In this research study, we investigate the impact of multiple exposure of individuals on the prevalence of COVID-19 and the efficacy of high-risk immunity measures in controlling its transmission dynamics. Through a qualitative analysis of a mathematical model, which includes the positivity of solutions, existence and uniqueness of solutions, and study of invariant regions, we demonstrate that the model can be utilized to examine pandemic outbreaks in a physical system. Our analysis of the basic reproductive ratio reveals that the implementation of high-risk immunity can reduce the number of secondary infections even in scenarios of multiple exposures. Numerical simulations, based on real-life COVID-19 data from the Nigeria center for disease control, were conducted using the homotopy perturbation method, yielding results that support the outcome of the basic reproductive ratio analysis and providing insight into strategies to mitigate the spread of the disease.

1. Introduction

The SARS-CoV-2 virus, responsible for the COVID-19 pandemic, rapidly spread globally, with initial outbreaks in Wuhan, China, in December 2019 [1]. By mid-July 2020, it had infected over 213 countries, resulting in millions of confirmed cases and hundreds of thousands of deaths [2]. The World Health Organization (WHO) confirmed respiratory droplets as a mode of transmission, leading to further infections [1]. The virus's incubation period ranges from 2 to 14 days, with approximately 97.5% of infected individuals exhibiting symptoms 11 days post-infection [1]. Del Rio and Malani's paper in 2020 provided new insights into the COVID-19 epidemic [1]. Though exact details aren't mentioned, it likely covered aspects like global spread, epidemiology, clinical presentation, and healthcare challenges [1]. Another paper discussed challenges posed by the closely related SARS-CoV, shedding light on unique COVID-19 characteristics [3]. A research article in 2020 focused on the early transmission dynamics of the virus in Wuhan [4]. It likely explored the initial spread and reproductive number (R_0) [4]. In 2021, a study proposed a fractional order model of COVID-19, considering the effects of fear induced by media and social networks on community behavior [5]. This model provides insights into the impact of human behavior on virus spread [5].

Several studies aimed at mitigating the spread of COVID-19 have been published by distinguished researchers and scientists. In particular, the study presented in [6] quantifies the fear impact of media exposure into two categories: fear of infection toll and fear of death toll, utilizing a mathematically formulated model. Another study [7] evaluated the impact of the convex incidence rate on the transmission dynamics of COVID-19 and

* Corresponding Author: mutairu.kolawole@uniosun.edu.ng

Received: April 16, 2023, Accepted: October 3, 2023

found that double exposure of vulnerable individuals could result in elevated rates of infection in the general population. A comprehensive assessment of COVID-19 transmission dynamics was conducted in [8], examining the effects of the convex incidence rate and proposing various strategies aimed at stabilizing the pace of disease reduction. The results showed that the dynamics of the disease are significantly influenced by factors such as immigration and population mixing in affected areas, leading to substantial decreases in infection rates.

High-risk immunity refers to a public health measure aimed at containing the spread of infectious diseases, such as COVID-19, by isolating individuals who are at elevated risk of transmitting the disease. This measure is usually implemented when an individual has been diagnosed with an infectious disease or has had close contact with someone who has been diagnosed. The goal of high-risk immunity is to prevent the infected individual from spreading the disease to others, thereby controlling the spread of the outbreak [9]. High-risk immunity is a crucial component of public health response strategies, particularly during pandemics, as it helps to reduce the transmission of the disease and slow down the spread of the outbreak. However, it can also have significant impacts on individuals and society, including loss of income, social isolation, and psychological distress. It is important for public health authorities to balance the benefits of high-risk immunity with its potential harms and to implement measures to mitigate the negative effects.

A convex incidence rate of disease occurs when the rate of disease or infection increases at a faster rate than it decreases [10]. This means that the rate of infection is increasing as time passes. The incidence rate of a disease or infection is the number of new cases per unit of time. Convex incidence rates can be caused by a variety of factors, such as the spread of a disease, the emergence of new strains, or a lack of access to treatment [11]. It can also be caused by environmental factors such as overcrowding and poor sanitation. Convex incidence rates can lead to a rapid increase in the number of cases of a disease or infection. This can have serious implications for public health, as more people may become ill, and the healthcare system may not be able to cope with the increasing demand. To prevent a convex incidence rate, it is important to identify the risk factors for a particular disease or infection and implement strategies to reduce these risk factors. This could include improving access to healthcare, providing education on preventive measures, or implementing control measures such as vaccinations.

The prediction of epidemic spread can be achieved through numerical simulations of epidemic models. To forecast the COVID-19 virus's progression, a mathematical model was constructed using real-world data from Pakistan, as described in [12]. A stochastic analysis of a COVID-19 model with effects of vaccination and different transition rates using real data approach was performed in [13]. The logistic growth model was evaluated in [14] as a potential method for determining the extent of the COVID-19 epidemic. In [15], a mathematical analysis of a stochastic model for coronavirus transmission, utilizing the Legendre collocation method, was performed and validated through simulations. Recent research [16] demonstrated the application of the Laplace-Adomian decomposition method in simulating fractional-order Caputo's derivative on a COVID-19 disease model and a study involving Lyapunov stability and wave analysis of Covid-19 omicron variant using real data with fractional operator was studied in [17]. Mathematical models often exhibit nonlinearity, necessitating the use of advanced numerical techniques for accurate solutions [18]. The homotopy perturbation method has been effectively utilized in various studies to solve complex nonlinear differential equations. For instance, in studies related to the EIAV infection epidemic [19] and the impact of disease transmission on the death seizure epidemic [20], the homotopy perturbation method provided valuable insights and solutions. Moreover, researchers have extended the use of the homotopy perturbation method to develop semi-analytical solutions for nonlinear models [17]. This modified approach allows for a more efficient and accurate solution to complex nonlinear problems. In addition to the homotopy perturbation method, other numerical techniques have also been employed in different modeling areas to solve classical and coupled systems of ordinary differential equations. Olayiwola et al. introduced an efficient algorithm for solving nonlinear partial differential equations [21]. Muideen et al. proposed an optimized three-step hybrid block method for stiff problems in ordinary differential equations [22]. Furthermore, a modified variational iteration method was employed for the solution of a class of differential equations [23]. The researchers Olayiwola, Gbolagade, and Akinpelu contributed to the field of mathematical physics with their work on approximate analytical methods for the solution of fractional-order integro-differential equations [13]. Their studies provide valuable insights into solving fractional-order equations, which have

applications in various scientific disciplines. In summary, the literature showcases various numerical methods, such as the homotopy perturbation method, variational iteration method, and hybrid block method, to address the challenges posed by nonlinear mathematical models. These methods have been instrumental in solving complex differential equations, providing researchers with valuable tools for understanding and analyzing real-world problems.

Several researchers, notably [8] and [10], have independently studied the application of convex incidence rates and high-risk immunity to the prevalence of COVID-19. As a subject of active research, we shall conduct an analysis of the impact of high-risk immunity on a proposed mathematical model that incorporates convex incidence rates, accounting for the rate of multiple COVID-19 exposures in the presence of vaccines, treatments, and curfews. Since such an analysis would require standard data and information as well as the application of advanced mathematical techniques, it is essential to accurately model the dynamic interactions between immunity measures, exposure risk, and the spread of the virus. We will conduct theoretical and qualitative analyses to establish the study's potential real-life applications and apply numerical simulations using results generated by the homotopy perturbation method with standard real-life and literature data through the modification of a mathematical model proposed in [24].

1.1. Basic Mathematical Model

$$\left. \begin{aligned} \frac{dS}{dt} &= \Lambda - \beta(1-w)SI(1+\alpha I) - \mu S \\ \frac{dE}{dt} &= \beta(1-w)SI(1+\alpha I) - (\mu + \gamma + \pi)E \\ \frac{dI}{dt} &= \pi E - (\delta + \mu + d)I \\ \frac{dQ}{dt} &= \delta I - (\mu + \theta)Q + \gamma E \\ \frac{dR}{dt} &= \theta Q - \mu R \end{aligned} \right\} \quad (1)$$

Subject to the following initial conditions

$$S(0) = s_0, \quad E(0) = e_0, \quad I(0) = i_0, \quad Q(0) = q_0, \quad R(0) = r_0 \geq 0.$$

1.2. Description of variables and parameters

From the model, $S(t)$ represents the population of susceptible individuals, i.e. those who are not infected with COVID-19 and can potentially contract the virus. $E(t)$ represents the population of exposed individuals, i.e. those who have been infected with COVID-19 but are not yet infectious. $I(t)$ represents population of infected individuals, i.e. those who have been infected with COVID-19 and are currently infectious. $Q(t)$ is the population of isolated individuals, i.e. those who have been infected with COVID-19 and are currently in quarantine or isolation. $R(t)$ stands for the population of recovered individuals, i.e. those who have been infected with COVID-19 and have recovered from the disease. w represents the high risk quarantine rate, i.e. the proportion of susceptible individuals who are quarantined due to their high risk of exposure to COVID-19 as a result of their existence in infected zone. α denotes the coefficient of multiple exposure of susceptible individuals to COVID-19. It is a measure of how likely susceptible individuals are to be exposed to COVID-19, based on factors such as their occupation, living conditions, and social interactions. Λ denotes the recruitment rate of individuals: it is the rate at which new individuals enter the susceptible population, e.g., through birth or immigration. β is the successful contact rate. It is the rate at which infected individuals come into contact with susceptible individuals and transmit the virus. π represents the progression rate from exposed to infectious: it is the rate at which exposed individuals become infected and become part of the infected population. σ is the progression rate from infected

to isolated class. It is the rate at which infected individuals are identified and quarantined. γ represents the progression rate from exposed to isolated class: it is the rate at which exposed individuals are identified and quarantined. θ is the recovery rate of isolated individual. It is the rate at which isolated individuals recover from COVID-19 and become part of the recovered population. The natural death rate is denoted by μ . It is the rate at which individuals in the population die from causes other than COVID-19.

Table 1: Description of parameters

VARIABLES	DEFINITION
$S(t)$	Population of susceptible individuals
$E(t)$	Population of exposed individuals
$I(t)$	Population of infected individuals
$Q(t)$	Population of isolated individuals
$R(t)$	Population of recovered individuals
INTRODUCED PARAMETERS	DEFINITION
w	High risk quarantine rate
α	Coefficient of multiple exposure of Susceptible individuals to COVID-19
Parameters	DESCRIPTION
Λ	Recruitment rate of Individuals
β	Successful contact rate
π	Progression rate from Exposed to Infected
σ	Progression rate from Infected to Isolated class
γ	Progression rate from Exposed to Isolated class
θ	Recovery rate of isolated individual
μ	Natural death rate

Table 2: Values of model’s parameter and references

Parameters	VALUE	REFERENCES
Λ	750 day^{-1}	[24]
β	0.0000124 day^{-1}	[24]
π	0.0000124 day^{-1}	[24]
σ	0.010939586 day^{-1}	[24]
γ	4.013000000 $\times 10^{-8} day^{-1}$	[24]
θ	0.0766169 day^{-1}	[24]
μ	0.001466848 day^{-1}	[24]
w	0	-
α	0	-

2. Model Analysis

2.1. Positivity and Boundedness of Solution

Consider the following classes of the system of equations given by:

$$\Omega = \{S(t), E(t), I(t), Q(t), R(t), \in \mathfrak{R}^5_+\}.$$

The total population at any time t is given by (1) and the derivatives obtained as;

$$\frac{dN(t)}{dt} = \frac{d}{dt}[S(t) + E(t) + I(t) + Q(t) + R(t)],$$

such that

$$\frac{dN(t)}{dt} = \frac{dS}{dt} + \frac{dE}{dt} + \frac{dI}{dt} + \frac{dQ}{dt} + \frac{dR}{dt},$$

$$\frac{dN(t)}{dt} = \Lambda - \mu(S + E + I + Q + R) - dI; \quad \frac{dN(t)}{dt} \leq \Lambda - \mu N;$$

Such that

$$\frac{dN(t)}{dt} + \mu N \leq \Lambda, \tag{2}$$

Which upon integration yields

$$N(t)e^{\mu t} = \frac{\Lambda}{\mu} e^{\mu t} + C.$$

$$\text{The time dependent number of human population is } N(t) = \frac{\Lambda}{\mu} + Ce^{-\mu t}, \tag{3}$$

Which is the birth and death ratio of human population. And as time progressively increases indefinitely i.e

$$t \rightarrow \infty \quad Ce^{-\mu t} = 0. \text{ Such that } N(t) \leq \frac{\Lambda}{\mu}.$$

This shows that it is sufficient to consider the dynamics of the model in \mathfrak{R}^5 which infers that the model is mathematically and epidemiologically well posed. Hence the nonnegative solution set of the model equations enters the feasible region, Ω , which is a positively invariant set.

2.2. Existence and Uniqueness of Solution

Let:

$$f_1 = \Lambda - \beta(1-w)SI(1+\alpha I) - \mu S$$

$$f_2 = \beta(1-w)SI(1+\alpha I) - (\mu + \gamma + \pi)E \tag{4}$$

$$f_3 = \pi E - (\delta + \mu + d)I$$

$$f_4 = \delta I - (\mu + \theta)Q + \gamma E$$

$$f_5 = \theta Q - \mu R$$

Then,

$$\begin{aligned} \left| \frac{df_1}{dS} \right| &= |\beta(1-w)(1+\alpha I) - \mu| < \infty, \quad \left| \frac{df_1}{dE} \right| = |0| < \infty, \quad \left| \frac{df_1}{dI} \right| = |\beta(1-w)(1+\alpha)| < \infty, \quad \left| \frac{df_1}{dQ} \right| = |0| < \infty, \quad \left| \frac{df_1}{dR} \right| = |0| < \infty \\ \left| \frac{df_2}{dS} \right| &= |\beta(1-w)(1+\alpha I) - \mu| < \infty, \quad \left| \frac{df_2}{dE} \right| = |(\mu + \gamma + \pi)| < \infty, \quad \left| \frac{df_2}{dI} \right| = |\beta(1-w)(1+\alpha)| < \infty, \quad \left| \frac{df_2}{dQ} \right| = |0| < \infty, \\ \left| \frac{df_2}{dR} \right| &= |0| < \infty \\ \left| \frac{df_3}{dS} \right| &= |0| < \infty, \quad \left| \frac{df_3}{dE} \right| = |\pi| < \infty, \quad \left| \frac{df_3}{dI} \right| = |(\delta + \mu + d)| < \infty, \quad \left| \frac{df_3}{dQ} \right| = |0| < \infty, \quad \left| \frac{df_3}{dR} \right| = |0| < \infty \\ \left| \frac{df_4}{dS} \right| &= |0| < \infty, \quad \left| \frac{df_4}{dE} \right| = |\delta| < \infty, \quad \left| \frac{df_4}{dI} \right| = |\gamma| < \infty, \quad \left| \frac{df_4}{dQ} \right| = |(\mu + \theta)| < \infty, \quad \left| \frac{df_4}{dR} \right| = |0| < \infty \\ \left| \frac{df_5}{dS} \right| &= |0| < \infty, \quad \left| \frac{df_5}{dE} \right| = |0| < \infty, \quad \left| \frac{df_5}{dI} \right| = |0| < \infty, \quad \left| \frac{df_5}{dQ} \right| = |\theta| < \infty, \quad \left| \frac{df_5}{dR} \right| = |\mu| < \infty \end{aligned}$$

The solution of the model is bounded, therefore is well-posed in \mathfrak{R}_5

2.3. Disease Free Equilibrium State

At disease free equilibrium point, there is no outbreak of disease. Therefore, $E = I = 0$. Thus equating the left hand side of (1) to zero, yields:

$$\begin{aligned} \Lambda - \beta(1-w)SI(1+\alpha I) - \mu S &= 0 \\ \beta(1-w)SI(1+\alpha I) - (\mu + \gamma + \pi)E &= 0 \\ \pi E - (\delta + \mu + d)I &= 0 \\ \delta I - (\mu + \theta)Q + \gamma E &= 0 \\ \theta Q - \mu R &= 0 \end{aligned} \tag{5}$$

Such that the disease-free equilibrium $(S_0, E_0, I_0, Q_0, R_0)$ is given by $\left(\frac{\Lambda}{\mu}, 0, 0, 0\right)$

2.4. Endemic Equilibrium Point

At endemic equilibrium, there is a persistence of disease in the system thus, $E \neq I \neq 0$. Let $E_e = (S^*, E^*, I^*, Q^*, R^*)$ be the endemic equilibrium of (1), and let,

$$g = \beta(1-w), \quad f = (\mu + \gamma + \pi), \quad e = (\mu + \delta + d), \quad j = \mu + \theta.$$

The endemic equilibrium points are obtained as:

$$S^* = \frac{\Lambda}{[(gI(1+\alpha I) + \mu)]}, \quad E^* = \frac{g}{f} \left[\frac{\pi}{gI(1+\alpha I) + \mu} \right], \quad I^* = \sqrt{\frac{(\alpha\Lambda - gf) + g\pi^2 - ef\mu}{gae f}}$$

$$Q^* = \frac{\delta gh p \pi \Lambda - e \mu \delta - \gamma \Lambda^2 e g h^2 \pi - e^2 \gamma \mu}{j(g h e f + e \mu)}, R^* = \frac{\theta \delta \Lambda g h p \pi - \theta e \mu \delta - \theta \gamma \Lambda^2 e g h^2 \pi e^2 \gamma \mu}{j \mu (g h e f + e \mu)}.$$

2.5. Basic Reproduction Number (R_0)

The model has three disease states, but only one causes new infections. This is represented by the connection between the exposed, infected and quarantined compartments in equation (1), which shows the number of secondary infections caused by infected individuals in the population. We apply the next generation matrix to obtain the basic reproductive ratio. Hence, consider:

$$\begin{aligned} \frac{dE}{dt} &= \beta(1-w)SI(1+\alpha I) - (\mu + \gamma + \pi)E, \\ \frac{dI}{dt} &= \pi E - (\delta + \mu + d)I, \\ \frac{dQ}{dt} &= \delta I - (\mu + \theta)Q + \gamma E. \end{aligned} \tag{6}$$

We create the following transition matrix

$$F_i = \left[\frac{\partial f_i(x_i)}{\partial x_j} \right] \text{ and } V_i = \left[\frac{\partial v_i(x_i)}{\partial x_j} \right] \text{ } i=1,2,3$$

which Jacobian yields:

$$F = \begin{bmatrix} 0 & \beta(1-w)S_0(1+\alpha) & 0 \\ 0 & 0 & 0 \\ 0 & 0 & 0 \end{bmatrix} \text{ and } V = \begin{bmatrix} (\mu + \gamma + \pi)E \\ -\pi E + (\delta + \mu + d)I \\ -\delta I + (\mu + \theta)Q - \gamma E \end{bmatrix}$$

Since $S_0 = \frac{\Lambda}{\mu}$, therefore

$$F = \begin{bmatrix} 0 & \frac{\beta(1-w)\Lambda(1+\alpha)}{\mu} & 0 \\ 0 & 0 & 0 \\ 0 & 0 & 0 \end{bmatrix}, V = \begin{bmatrix} (\mu + \gamma + \pi) & 0 & 0 \\ -\pi & (\mu + d + \delta) & 0 \\ -\gamma & -\delta & (\mu + \theta) \end{bmatrix}$$

$$\text{and } V^{-1} = \begin{bmatrix} \frac{1}{(\mu + \gamma + \pi)} & 0 & 0 \\ \frac{\pi(\mu + \theta)}{(\mu + \gamma + \pi)(\mu + \delta + d)(\mu + \theta)} & \frac{1}{(\mu + \delta + d)} & 0 \\ \frac{\pi\delta + \gamma(\mu + \delta + d)}{(\mu + \gamma + \pi)(\mu + \delta + d)(\mu + \theta)} & \frac{-\delta}{(\mu + \delta + d)(\mu + \theta)} & \frac{1}{(\mu + \theta)} \end{bmatrix}.$$

The required R_0 is the spectral radius of matrix $|G - \lambda I| = 0$ where $G = F \times V^{-1}$.

Hence, the basic reproductive ratio is:

$$R_0 = \frac{\beta\Lambda\pi(1-w)(1+\alpha)}{\mu(\mu+\gamma+\pi)(\mu+\delta+d)} \tag{7}$$

2.5.1. Analysis of the Basic reproductive ratio R_0

Here, the significant effect of the incorporated parameters is examined on the basic reproductive ratio. We initiate the step by evaluating the R_0 using the baseline parameters on Table 2. The proceedings of the evaluation yields $R_0 = 2.204147669(1-w)(1+\alpha)$

Table 3: Effect of Induced parameters on R_0

Rate of w	effect on R_0	Rate of α	effect on R_0	Combined Rate of w, α	Simultaneous effect on R_0
$w = 0, \alpha = 0$	2.204147669	$w = 0, \alpha = 0$	2.204147669	$w = 0, \alpha = 0$	2.204147669
$w = 0.3, \alpha = 0$	1.542903369	$w = 0, \alpha = 0.3$	2.865391970	$w = 0.3, \alpha = 0.3$	2.005774379
$w = 0.6, \alpha = 0$	0.8816590677	$w = 0, \alpha = 0.6$	3.526636271	$w = 0.6, \alpha = 0.6$	1.410654509
$w = 0.9, \alpha = 0$	0.2204147669	$w = 0, \alpha = 0.9$	4.187880571	$w = 0.9, \alpha = 0.9$	0.4187880571

Table 3 shows the impact of the two factors on R_0 . The initial examination illustrates that elevating the degree of High-risk immunity exerts a noteworthy influence on the basic reproductive number R_0 . Conversely, a rise in the value of the multiple exposure factor results in an elevation of R_0 , signifying that without an adequate plan in place for individuals who do not follow the curfew regulation, the system may become destabilized as every person will eventually be contaminated. The concurrent evaluation of both variables on R_0 reveals that even in cases of recurrent COVID-19 exposures, R_0 would still decrease with maximum implementation of High-risk immunity.

2.6. Local Stability of Disease Free Equilibrium

The local stability of the disease-free equilibrium suggests that a small number of infected individuals introduced into a disease-free population will not cause a major outbreak, and the infection will eventually die out. However, this does not ensure long-term absence of the disease, as larger perturbations or parameter changes could still lead to an outbreak. For long-term eradication of the disease, global stability is necessary. The Disease-Free Equilibrium (DFE) of the proposed Epidemic Model is locally asymptotically stable if $R_0 < 1$ and unstable if

$R_0 > 1$. The local stability of the disease-free equilibrium at $(S, E, I, Q, R) = \left(\frac{\Lambda}{\mu}, 0, 0, 0, 0\right)$

The Jacobian matrix of the system (1) is obtained, and the characteristic polynomial obtained using $|J_{E_1} - \lambda_i I| = 0$ will be solved to obtain the eigen-values $\lambda_i, i = 1, 2, \dots, 5$. Hence,

$$J_{(E_1)} = \begin{pmatrix} -\mu & 0 & -\frac{\beta\Lambda(1-w)(1+\alpha)}{\mu} & 0 & 0 \\ 0 & -(\mu+\gamma+\pi) & \frac{\beta\Lambda(1-w)(1+\alpha)}{\mu} & 0 & 0 \\ 0 & \pi & -(\delta+\mu+d) & 0 & 0 \\ 0 & \gamma & \delta & -(\mu+\theta) & 0 \\ 0 & 0 & 0 & \theta & -\mu \end{pmatrix} \tag{8}$$

and $|J_{E_1} - \lambda_i I| = 0$ implies

$$\begin{vmatrix} -\mu - \lambda_1 & 0 & -\frac{\beta\Lambda(1-w)(1+\alpha)}{\mu} & 0 & 0 \\ 0 & -(\mu+\gamma+\pi) - \lambda_2 & \frac{\beta\Lambda(1-w)(1+\alpha)}{\mu} & 0 & 0 \\ 0 & \pi & -(\delta+\mu+d) - \lambda_3 & 0 & 0 \\ 0 & \gamma & \delta & -(\mu+\theta) - \lambda_4 & 0 \\ 0 & 0 & 0 & \theta & -\mu - \lambda_5 \end{vmatrix} = 0$$

Such that we obtain

$$\lambda_1 = -\mu, \lambda_2 = -\frac{1}{2\mu} \left(2\mu^2 + \mu\delta + \mu\delta + \mu\gamma + \mu\pi + \sqrt{\begin{matrix} \mu^2\delta^2 + \mu^2\pi^2 + \mu^2\gamma^2 + \mu^2d^2 \\ -2\mu^2\delta\pi + 2\mu^2\delta d - 2\mu^2\delta\gamma \\ -2\mu^2\gamma d + 2\mu^2\pi d + 2\mu^2\pi\gamma \\ -2\gamma\mu^2 d + 4\mu\beta\Lambda\pi d - 4\mu\beta\Lambda\pi w \end{matrix}} \right)$$

$$\lambda_3 = -\frac{1}{2\mu} (2\mu^2 + \mu\delta + \mu d + \mu\gamma + \mu\pi) + \sqrt{\begin{matrix} \mu^2\delta^2 + \mu^2\pi^2 + \mu^2\gamma^2 + \mu^2d^2 \\ -2\pi\gamma\mu^2 + 2\delta\mu^2 d - 2\delta\mu^2\gamma \\ -2\pi d\mu^2 + 2\pi\gamma\mu^2 - 2\pi d\mu^2 \\ +4\pi\beta\mu\Lambda - 4\pi\beta\mu\Lambda w \end{matrix}}$$

$$\lambda_4 = -(\theta + \mu), \lambda_5 = -\mu$$

All the obtained eigen values are negative, therefore system (1) is Locally Asymptotically Stable. Therefore the disease will eventually die out in the system.

2.7. Local Stability of Endemic Equilibrium

The endemic equilibrium of the proposed mathematical Model is locally asymptotically stable if $R_0 < 1$ and unstable otherwise. We apply the linearization technique to prove this. Hence, to linearize the mathematical model, we substitute the following parameters $S = x + S^*$, $E = y + E^*$, $I = z + I^*$, $Q = p + Q^*$, $R = q + R^*$ into (1) yields

$$\left. \begin{aligned} \frac{dx}{dt} &= \Lambda - \beta(1-w)(x+S^*)(z+I^*)(1+\alpha(z+I^*)) - \mu(x+S^*) \\ \frac{dy}{dt} &= \beta(1-w)(x+S^*)(z+I^*)(1+\alpha(z+I^*)) - (\mu+\gamma+\pi)(y+E^*) \\ \frac{dz}{dt} &= \pi(y+E^*) - (\delta+\mu+d)(z+I^*) \\ \frac{dp}{dt} &= \delta(z+I^*) - (\mu+\theta)(p+Q^*) + \gamma(y+E^*) \\ \frac{dq}{dt} &= \theta(p+Q^*) - \mu(q+R^*) \end{aligned} \right\} \tag{9}$$

Such that we have

$$\begin{aligned} \frac{dx}{dt} &= -\beta(1-w)(1+\alpha z)xz - \mu x + \text{higher order nonlinear terms} \\ \frac{dy}{dt} &= \beta(1-w)(1+\alpha z)xz - \mu x - (\mu+\gamma+\pi)y + \text{higher order nonlinear terms} \\ \frac{dz}{dt} &= \pi y - (\delta+\mu+d)z + \text{higher order nonlinear terms} \\ \frac{dp}{dt} &= \delta z - (\mu+\theta)p + \gamma y + \text{higher order nonlinear terms} \\ \frac{dq}{dt} &= \theta p - \mu q + \text{higher order nonlinear terms} \end{aligned}$$

The Jacobian matrix of the system is:

$$J_{E^*} = \begin{vmatrix} -[\beta(1-w)(1+\alpha z)z + \mu] & 0 & \beta(1-w)(1+\alpha)x & 0 & 0 \\ \beta(1-w)(1+\alpha z)z - \mu & -(\mu+\gamma+\pi) & \beta(1-w)(1+\alpha z)x & 0 & 0 \\ 0 & \pi & -(\delta+\mu+d) & 0 & 0 \\ 0 & \gamma & \delta & -(\mu+\theta) & 0 \\ 0 & 0 & 0 & \theta & -\mu \end{vmatrix} \tag{10}$$

Such that the characteristic polynomial $|J_{E_i} - \lambda_i I| = 0$ yields:

$$\begin{vmatrix} -[\beta(1-w)(1+\alpha z)z + \mu] - \lambda & 0 & \beta(1-w)(1+\alpha)x & 0 & 0 \\ \beta(1-w)(1+\alpha z)z - \mu & -(\mu+\gamma+\pi) - \lambda & \beta(1-w)(1+\alpha z)x & 0 & 0 \\ 0 & \pi & -(\delta+\mu+d) - \lambda & 0 & 0 \\ 0 & \gamma & \delta & -(\mu+\theta) - \lambda & 0 \\ 0 & 0 & 0 & \theta & -\mu - \lambda \end{vmatrix} = 0$$

The resulting eigen-values are:

Let $A = -[\beta(1-w)(1+\alpha z)z + \mu]$, $B = -(\mu + \gamma + \pi)$, $C = -(\delta + \mu + d)$, $D = -(\mu + \theta)$, $E = -\mu$

We have

$$(A - \lambda)(B - \lambda)(C - \lambda)(D - \lambda)(E - \lambda) = 0 \quad (11)$$

Equation (11) that the system is locally asymptotically stable. Thus, this also assures that the disease will eventually be wiped out as time progresses.

2.8. Global Stability of Disease-Free Equilibrium

Here we construct a Lyapunov function approach to proceed for the result for Global Asymptotic Stability of the proposed model, at Disease Free Equilibrium State. Hence we have:

$$\frac{dE}{dt} = \beta(1-w)SI(1+\alpha I) - (\mu + \gamma + \pi)E$$

$$\frac{dI}{dt} = \pi E - (\delta + \mu + d)I$$

$$\frac{dQ}{dt} = \delta I - (\mu + \theta)Q + \gamma E$$

$$\Omega = \left\{ E(t), I(t), Q(t), \in \mathfrak{R}^3_+ : N \leq \frac{\Lambda}{\mu} \right\}$$

$$V(t, S, E, I, Q, R) = C_1 I_1 + C_2 I_2 + C_3 I_3$$

$$\frac{dV}{dt} = C_1 I_1^* + C_2 I_2^* + C_3 I_3^*$$

$$= C_1 [\beta(1-w)S_0 I_2 (1 + \alpha I_2) - (\mu + \gamma + \pi)I_1] + C_2 [\pi I_1 - (\delta + \mu + d)I_2] + C_3 [\delta I_2 - (\mu + \theta)I_3 + \gamma I_1]$$

$$= C_1 \beta(1-w)S_0 I_2 (1 + \alpha I_2) - C_1 (\mu + \gamma + \pi)I_1 + C_2 \pi I_1 - C_2 (\delta + \mu + d)I_2 + C_3 \delta I_2 - C_3 (\mu + \theta)I_3 + C_3 \gamma I_1$$

$$\leq [C_2 \pi - C_1 (\mu + \gamma + \pi) + C_3 \gamma] I_1 + [C_1 \beta(1-w)S_0 (1 + \alpha) - C_2 (\delta + \mu + d) + C_3 \delta] I_2 - [C_3 (\mu + \theta)] I_3$$

$$\leq [C_2 \pi - C_1 (\mu + \gamma + \pi) + C_3 \gamma] I_1 + \left[C_1 \frac{\beta \Lambda (1-w)(1+\alpha)}{\mu} - C_2 (\delta + \mu + d) + C_3 \delta \right] I_2 - [C_3 (\mu + \theta)] I_3 \leq N, S$$

$$\text{As } S_0 = \frac{\Lambda}{\mu}, \text{ Let } C_1 = \frac{1}{(\mu + \gamma + \pi)(\delta + \mu + d)}, C_2 = \frac{\beta \Lambda (1-w)(1+\alpha)}{\mu(\mu + \gamma + \pi)(\delta + \mu + d)}, C_3 \leq 0$$

$$\leq (\delta + \mu + d) \left[\frac{\beta \Lambda (1-w)(1+\alpha)\pi}{\mu(\mu + \gamma + \pi)(\delta + \mu + d)^2} - \frac{(\mu + \gamma + \pi)}{(\mu + \gamma + \pi)(\delta + \mu + d)} \right] I_1 \\ + \left[\frac{\beta \Lambda (1-w)(1+\alpha)}{\mu(\mu + \gamma + \pi)(\delta + \mu + d)} - \frac{\beta \Lambda (1-w)(1+\alpha)(\delta + \mu + d)}{\mu(\mu + \gamma + \pi)(\delta + \mu + d)^2} \right] I_2$$

$$V^* \leq \left[\frac{\beta\Lambda(1-w)(1+\alpha)\pi}{\mu(\mu+\gamma+\pi)(\delta+\mu+d)} - 1 \right] I$$

$$V^\bullet \leq [R_0 - 1]I$$

It is imperative to note that $V^\bullet = 0$ only when $E = 0$, the substitution of $E = 0$ into the model system of equation (1) shows that $S_0 = \frac{\Lambda}{\mu}$ at $t \rightarrow \infty$. Based on LaSalle’s invariance principle of model stability. Hence $E_0 = 0$ is globally asymptotically Stable whenever $R_0 < 1$

2.9. Sensitivity analysis of R_0

We are to test for the sensitivity of R_0 by differentiating R_0 with respect to all the parameters in R_0 . The normalized forward sensitivity index is defined:

$$\text{As } R_0 = \frac{\beta\Lambda\pi(1-w)(1+\alpha)}{\mu(\mu+\gamma+\pi)(\mu+\delta+d)}$$

Tabular representation of parameter and indices of sensitivity analysis is deduced from the initial values of the said parameters.

Table: Parameter and indices sensitivity analysis

Parameter	Sensitivity
Λ	1
β	1
π	0
σ	0
γ	0
μ	-2.748752009
w	0
α	0

3. Homotopy perturbation method

An objective of this study is to undertake numerical simulations of a mathematical model through the development of an approximation solution. This objective is being achieved by utilizing the homotopy perturbation method. An in-depth examination of this technique will be presented by analyzing the following differential equation.

$$\Delta(\omega) = k(r), \quad r \in \Phi. \tag{12}$$

Subject to the boundary condition

$$\Psi(\omega, \omega_n) = 0 \quad r \in \Pi. \tag{13}$$

Operator Δ denotes the differential operator, the boundary operator is Ψ , $k(r)$ is an analytic function, the boundary of the domain Φ is denoted by Π , and ω_n is the normal vector derivative drawn externally from Φ .

We can split the operator $\Delta(\omega)$ into two parts such that

$$\Delta(\omega) = L_T(\omega) + N_T(\omega), \tag{14}$$

The operator $L_T(\omega)$, $N_T(\omega)$ denotes the linear and nonlinear term respectively such that equation (14) implies.

$$L_T(\omega) + N_T(\omega) = k(r), \quad r \in \Phi. \quad (15)$$

We can construct a Homotopy for (15) so that

$$H(f, p) = (1 - p)[L_T(f) - L_T(\omega_0)] + p[\Delta(f) - k(r)] = 0. \quad (16)$$

Where p is an embedding parameter which can undergo a deformation process of changing from $[0,1]$. Equation (16) is further simplified to obtain:

$$H(f, p) = L_T(f) - L_T(\omega_0) + p[L_T(\omega_0)] + p[N_T(\omega_0) - k(r)] = 0, \quad (17)$$

as $p \rightarrow 0$, equation (17) gives:

$$H(f, 0) = L_T(f) - L_T(\omega_0) = 0 \quad (18)$$

And when $p \rightarrow 1$,

$$H(f, 1) = \Delta(f) - k(r) = 0. \quad (19)$$

We can naturally assume the solution (12) as a power series such that

$$f(t) = f_0(t) + pf_1(t) + p^2 f_2(t) + \dots + p^n f_n(t) \quad (20)$$

Evaluating (19) with (20), and comparing coefficients of equal powers of p .

The values of $f_0(t)$, $f_1(t)$, $f_2(t)$ are obtained by solving the resulting ordinary differential equations. Thus, the approximate solution of (25) is:

$$f(t) = \lim_{p \rightarrow 1} f_n(t) = f_0(t) + f_1(t) + f_2(t) + \dots \quad (21)$$

3.1. Numerical Solution

In this part, we use the homotopy perturbation approach to conduct the numerical simulation that produces the SEIQR epidemic model's approximate solution. Constructing a homotopy for (1),

$$\begin{aligned} (1-p) \frac{dS(t)}{dt} + p \left(\frac{dS(t)}{dt} - (\Lambda - \beta(1-c)S(t)I(t)(1+\alpha I) - \mu S(t)) \right) &= 0, \\ (1-p) \frac{dE(t)}{dt} + p \left(\frac{dE(t)}{dt} - (\beta(1-c)S(t)I(t)(1+\alpha I) - (\mu + \gamma + \pi)E(t)) \right) &= 0, \\ (1-p) \frac{dI(t)}{dt} + p \left(\frac{dI(t)}{dt} - (\pi E(t) - (d + \mu + \delta)I(t)) \right) &= 0, \\ (1-p) \frac{dQ(t)}{dt} + p \left(\frac{dQ(t)}{dt} - (\gamma E(t) + \delta I(t) - (\theta + \mu)Q(t)) \right) &= 0, \\ (1-p) \frac{dR(t)}{dt} + p \left(\frac{dR(t)}{dt} - (\theta Q(t) - \mu R(t)) \right) &= 0. \end{aligned} \quad (22)$$

The approximate solution of (1) can be assumed as:

$$\begin{aligned}
S(t) &= s_0(t) + ps_1(t) + p^2s_2(t) + \dots p^n s_n(t) \\
E(t) &= e_0(t) + pe_1(t) + p^2e_2(t) + \dots p^n s_n(t) \\
I(t) &= i_0(t) + pi_1(t) + p^2i_2(t) + \dots p^n s_n(t) \\
Q(t) &= q_0(t) + pq_1(t) + p^2q_2(t) + \dots p^n s_n(t) \\
R(t) &= r_0(t) + pr_1(t) + p^2r_2(t) + \dots p^n s_n(t)
\end{aligned} \tag{23}$$

Substituting (34) into (33) and comparing coefficients of equal powers of p ,

$$p^0: \quad \dot{i}_0(t) = 0, \quad \dot{e}_0(t) = 0, \quad \dot{i}_0(t) = 0, \quad \dot{q}_0(t) = 0, \quad \dot{r}_0(t) = 0, \tag{24}$$

Solving (36) yields

$$s_0(t) = s_0, \quad e_0(t) = e_0, \quad i_0(t) = i_0, \quad q_0(t) = q_0, \quad r_0(t) = r_0 \tag{25}$$

Similarly comparing the coefficients of p^1 ,

$$\begin{aligned}
\frac{dS_1(t)}{dt} &= \Lambda - \beta(1-w)S_0(t)I_0(t)(1+\alpha I_0) - \mu S_0(t), \\
\frac{dE_1(t)}{dt} &= \beta(1-w)S_0(t)I_0(t)(1+\alpha I_0) - (\mu + \gamma + \pi)E_0(t), \\
\frac{dI_1(t)}{dt} &= \pi E_0(t) - (d + \mu + \delta)I_0(t), \\
\frac{dQ_1(t)}{dt} &= \gamma E_0(t) + \delta I_0(t) - (\theta + \mu)Q_0(t), \\
\frac{dR_1(t)}{dt} &= \theta Q_0(t) - \mu R_0(t)
\end{aligned} \tag{26}$$

Evaluating (37) using (36), and then solving the resulting system of equations, produces;

$$\begin{aligned}
S_1(t) &= (\Lambda - \beta(1-w)S_0(t)I_0(t)(1+\alpha I_0) - \mu S_0(t))t \\
E_1(t) &= (\beta(1-w)S_0(t)I_0(t)(1+\alpha I_0) - (\mu + \gamma + \pi)E_0(t))t \\
I_1(t) &= (\pi E_0(t) - (d + \mu + \delta)I_0(t))t \\
Q_1(t) &= (\gamma E_0(t) + \delta I_0(t) - (\theta + \mu)Q_0(t))t \\
R_1(t) &= (\theta Q_0(t) - \mu R_0(t))t
\end{aligned} \tag{27}$$

The coefficients of p^2 equally yields:

$$\begin{aligned}
 \frac{dS_2(t)}{dt} &= \Lambda - \beta(1-w)S_1(t)I_1(t)(1+\alpha I_1) - \mu S_1(t), \\
 \frac{dE_2(t)}{dt} &= \beta(1-w)S_1(t)I_1(t)(1+\alpha I_1) - (\mu + \gamma + \pi)E_1(t), \\
 \frac{dI_2(t)}{dt} &= \pi E_1(t) - (d + \mu + \delta)I_1(t), \\
 \frac{dQ_2(t)}{dt} &= \gamma E_1(t) + \delta I_1(t) - (\theta + \mu)Q_1(t), \\
 \frac{dR_2(t)}{dt} &= \theta Q_1(t) - \mu R_1(t)
 \end{aligned}
 \tag{28}$$

The second Approximation are obtained by solving these equations.

The second Approximations are

$$\begin{aligned}
 s_2(t) &= \frac{1}{2}t^2 \left(\begin{aligned} &\beta di_0s_0 + \beta \delta_0s_0 + 3\beta \mu i_0s_0 + \beta^2 i_0^2s_0 - \Lambda \beta i_0 - \pi \beta e_0s_0 + \mu^2s_0 - \Lambda \mu \\ &+ \pi \beta we_0s_0 + \alpha^2 \beta^2 i_0^4s_0 + 2\alpha \beta^2 i_0^3s_0 - \Lambda \alpha \beta i_0^2 + \beta^2 w^2 i_0^2s_0 - 2\beta^2 wi_0^2s_0 \\ &+ \Lambda \beta wi_0 - 4\alpha \beta \mu wi_0^2s_0 - 2\alpha \beta d wi_0^2s_0 - 2\alpha \beta \delta wi_0^2s_0 + 2\pi \alpha \beta we_0i_0s_0 - 2\pi \alpha \beta e_0i_0s_0 \\ &+ \alpha^2 \beta^2 w^2 i_0^4s_0 - 2\alpha^2 \beta^2 wi_0^4s_0 + 2\alpha \beta^2 w^2 i_0^3s_0 - 4\alpha \beta^2 wi_0^3s_0 + \Lambda \alpha \beta wi_0^2 + 2\alpha \beta di_0^2s_0 \\ &+ 2\alpha \beta \delta_0^2s_0 + 4\alpha \beta \mu i_0^2s_0 - \beta d wi_0s_0 - \beta \delta wi_0s_0 - 3\beta \mu wi_0s_0 \end{aligned} \right) \\
 e_2(t) &= -\frac{1}{2}t^2 \left(\begin{aligned} &-\gamma \alpha \beta wi_0^2s_0 - \pi \alpha \beta wi_0^2s_0 - \gamma \beta wi_0s_0 + \pi \alpha \beta^2s_0 - \pi \beta wi_0s_0 + \gamma \alpha \beta^2s_0 - \gamma^2e_0^2 - \pi^2e_0 - 2\gamma \mu e_0 \\ &- 2\pi \mu e_0 + \mu^2e_0 - 2\gamma \pi e_0 + \beta di_0s_0 + \beta \delta_0s_0 + 3\beta \mu i_0s_0 + \pi \beta i_0s_0 + \gamma \beta i_0s_0 + \beta^2 i_0^2s_0 - \Lambda \beta i_0 \\ &+ \alpha^2 \beta^2 i_0^4s_0 + 2\alpha \beta^2 i_0^3s_0 - \Lambda \alpha \beta^2 i_0^2 + \beta^2 w^2 i_0^2s_0 - 2\beta^2 wi_0^2s_0 - \pi \beta e_0s_0 + \pi \beta we_0s_0 \\ &+ \Lambda \beta wi_0 - 4\alpha \beta \mu wi_0^2s_0 - 2\alpha \beta d wi_0^2s_0 - 2\alpha \beta \delta wi_0^2s_0 + 2\alpha \pi \beta wi_0s_0 - 2\alpha \pi \beta e_0i_0s_0 + \alpha^2 \beta^2 w^2 i_0^4s_0 \\ &- 2\alpha^2 \beta^2 wi_0^4s_0 + 2\alpha \beta^2 w^2 i_0^3s_0 - 4\alpha \beta^2 wi_0^3s_0 + \Lambda \alpha \beta wi_0^2 + 2\alpha \beta di_0^2s_0 + 2\alpha \beta \delta_0^2s_0 \\ &+ 4\alpha \beta \mu i_0^2s_0 - \beta d wi_0s_0 - \beta \delta wi_0s_0 - 3\beta \mu wi_0s_0 \end{aligned} \right) \\
 i_2(t) &= -\frac{1}{2}t^2 \left(\begin{aligned} &\pi \alpha \beta wi_0^2s_0 - \pi \alpha \beta^2s_0 + \pi \beta wi_0s_0 - \pi \beta i_0s_0 + \pi^2e_0 + \pi d e_0 + \pi \delta_0 \\ &+ \pi \gamma e_0 + 2\pi \mu e_0 - d^2i_0 - 2d \delta_0 - 2d \mu i_0 - \delta^2i_0 - 2\delta \mu i_0 - \mu^2i_0 \end{aligned} \right) \\
 q_2(t) &= -\frac{1}{2}t^2 \left(\begin{aligned} &\alpha \beta \gamma wi_0^2s_0 - \alpha \beta \gamma i_0^2s_0 + \beta \gamma wi_0s_0 - \beta \gamma i_0s_0 - \pi \delta_0 + \pi \gamma e_0 + d \delta_0 \\ &+ \delta^2i_0 + 2\delta \mu i_0 + \delta \theta_0 + \gamma^2e_0 + 2\gamma \mu e_0 + \gamma \theta e_0 - \mu^2q_0 - 2\mu \theta q_0 - \theta^2q_0 \end{aligned} \right) \\
 r_2(t) &= \frac{1}{2}t^2 (\delta \theta_0 + \gamma \theta e_0 + \mu^2r_0 - 2\mu \theta q_0 - \theta^2q_0)
 \end{aligned}$$

4. Results

Here, we obtain the solutions of each class by taking the sum of their partial iterations hence, we have:

$$S(t) = \sum_{n=0}^4 s_n(t), \quad E(t) = \sum_{n=0}^4 e_n(t), \quad I(t) = \sum_{n=0}^4 i_n(t), \quad Q(t) = \sum_{n=0}^4 q_n(t), \quad R(t) = \sum_{n=0}^4 r_n(t).$$

To study the impact of the incorporated parameters on the mathematical model, we evaluated the obtained results using the following COVID-19 data of Lagos acquired from the Nigeria center for disease control on 1st December 2020 [19] presented as $E(0) = 2003$, $I(0) = 416$, $Q(0) = 404$, $R(0) = 115$. The current population of Ikeja, Lagos Nigeria is applied as the susceptible population [24] $S(0) = 470200$ such that the evaluated results yield the following series results containing the parameters whose influences are to be examined.

$$S(t) = 470200 + \left(1.008999547 \times 10^6 \alpha w - 1.008999547 \times 10^6 \alpha + 2425.479680w - 3238.700958 \right) t$$

$$+ \frac{1}{2} t^2 \left(\begin{aligned} &2.165206478 \times 10^6 \alpha^2 + 12.51159438w^2 + 76.44829437 + 56255.96956\alpha - 86.25626306w \\ &- 66665.61608\alpha w - 4.330412956 \times 10^6 \alpha^2 w + 10409.64652\alpha w^2 + 2.165206478 \times 10^6 \alpha^2 w^2 \end{aligned} \right)$$

$$+ \frac{1}{6} t^3 \left(\begin{aligned} &3.625743584w - 3265.211544\alpha + 4664.412242\alpha w + 7.751645814 \times 10^5 \alpha^2 w - 1479.746380\alpha w^2 \\ &- 4.378427956 \times 10^5 \alpha^2 w^2 + 80.54568096w^3 \alpha + 33507.00327w^3 \alpha^2 + 1.303891336 \times 10^7 \alpha^3 w \\ &+ 4.646304455 \times 10^6 \alpha^3 w^3 - 1.393891336 \times 10^7 \alpha^2 w^3 - 3.708287891 \times 10^5 \alpha^2 - 1.220637838w^2 \\ &- 4.646304455 \times 10^6 \alpha^3 + 0.06453980844w^3 - 2.478633996 \end{aligned} \right)$$

$$- \frac{1}{24} t^4 \left(\begin{aligned} &0.1770978022w - 203.2373146\alpha + 346.1973798\alpha w + 1.044528951 \times 10^5 \alpha^2 w - 165.6268025\alpha w^2 \\ &69845.87057\alpha^2 w^2 + 23.22071970\alpha^3 w + 12207.19453\alpha^3 w^2 + 5.754421783 \times 10^6 \alpha^3 w \\ &+ 2.173793894 \times 10^6 \alpha^3 w^3 - 5.946161758 \times 10^6 \alpha^3 w^2 - 5.982287227 \times 10^7 \alpha^4 w^2 \\ &- 9.970478712 \times 10^6 \alpha^4 w^4 + 3.988191485 \times 10^7 \alpha^3 w^4 + 3.988191485 \times 10^7 \alpha^4 w \\ &- 0.5539824544w^4 \alpha - 95896.98760\alpha^2 w^4 - 46468.53488\alpha^2 - 0.09375716092w^2 - 0.09718119346 \\ &- 1.886183932 \times 10^6 \alpha^3 + 0.01414359139w^3 - 9.970478712 \times 10^6 \alpha^4 - 0.0003329221480w^4 \end{aligned} \right)$$

$$E(t) = 2003 + \left(-1.008999547 \times 10^6 \alpha w - 1.008999547 \times 10^6 \alpha + 2425.479680w - 3238.700958 \right) t$$

$$+ \frac{1}{2} t^2 \left(\begin{aligned} &2.165206478 \times 10^6 \alpha^2 + 12.51159438w^2 + 76.44829437 + 56255.96956\alpha - 86.25626306w \\ &- 66665.61608\alpha w - 4.330412956 \times 10^6 \alpha^2 w + 10409.64652\alpha w^2 + 2.165206478 \times 10^6 \alpha^2 w^2 \end{aligned} \right)$$

$$+ \frac{1}{6} t^3 \left(\begin{aligned} &3.625743584w - 3265.211544\alpha + 4664.412242\alpha w + 7.751645814 \times 10^5 \alpha^2 w - 1479.746380\alpha w^2 \\ &- 4.378427956 \times 10^5 \alpha^2 w^2 + 80.54568096w^3 \alpha + 33507.00327w^3 \alpha^2 + 1.303891336 \times 10^7 \alpha^3 w \\ &+ 4.646304455 \times 10^6 \alpha^3 w^3 - 1.393891336 \times 10^7 \alpha^2 w^3 - 3.708287891 \times 10^5 \alpha^2 - 1.220637838w^2 \\ &- 4.646304455 \times 10^6 \alpha^3 + 0.06453980844w^3 - 2.478633996 \end{aligned} \right)$$

$$- \frac{1}{24} t^4 \left(\begin{aligned} &0.1770978022w - 203.2373146\alpha + 346.1973798\alpha w + 1.044528951 \times 10^5 \alpha^2 w - 165.6268025\alpha w^2 \\ &69845.87057\alpha^2 w^2 + 23.22071970\alpha^3 w + 12207.19453\alpha^3 w^2 + 5.754421783 \times 10^6 \alpha^3 w \\ &+ 2.173793894 \times 10^6 \alpha^3 w^3 - 5.946161758 \times 10^6 \alpha^3 w^2 - 5.982287227 \times 10^7 \alpha^4 w^2 \\ &- 9.970478712 \times 10^6 \alpha^4 w^4 + 3.988191485 \times 10^7 \alpha^3 w^4 + 3.988191485 \times 10^7 \alpha^4 w \\ &- 0.5539824544w^4 \alpha - 95896.98760\alpha^2 w^4 - 46468.53488\alpha^2 - 0.09375716092w^2 \\ &- 1.886183932 \times 10^6 \alpha^3 + 0.01414359139w^3 - 9.970478712 \times 10^6 \alpha^4 \\ &- 0.0003329221480w^4 - 0.0971811935 \end{aligned} \right)$$

$$I(t) = 416 - 8.399725754t - \frac{1}{2} t^2 (11.72255674\alpha w - 11.72255674\alpha + 0.02817922292w - 0.1981757720)$$

$$- \frac{1}{6} t^3 \left(\begin{aligned} &0.004869416444 - 1.012011290\alpha w - 50.31073772\alpha^2 w + 0.8910720168\alpha + 0.0001453597035w^2 \\ &+ 25.1553688\alpha^2 + 0.1209392734w^2 \alpha + 25.1553688\alpha^2 w^2 - 0.001573015077w \end{aligned} \right)$$

$$+ \frac{1}{24} t^4 \left(\begin{aligned} &- 0.00007398642906w - 0.05598536228\alpha - 0.07469141452\alpha w - 10.02511972\alpha^2 w + 0.01964183195\alpha w^2 \\ &+ 5.596486407\alpha^2 w^2 - 0.000935779721\alpha w^3 - 0.3892843641\alpha^2 w^3 - 161.9422954\alpha^3 w \\ &- 53.98076514\alpha^3 w^3 + 161.9422954\alpha^3 w^2 + 4.817917679\alpha^2 + 0.000017126484w^2 + 53.98076514\alpha^2 \\ &- 7.498234947 \times 10^{-7} w^3 + 0.0001272965002 \end{aligned} \right)$$

$$\begin{aligned}
 Q(t) = & 404 - 31.4962177t - \frac{1}{2}t^2(0.04049115182\alpha w - 0.04049115182\alpha + 0.00009733449956w - 2.501806504) \\
 & - \frac{1}{6}t^3 \left(\begin{aligned} & 0.1996200021 + 0.01662979047\alpha w + 0.1737794719\alpha^2 w - 0.01704752958\alpha + 0.0001453597035w^2 \\ & + 5.020902824 \times 10^{-7} w^2 + 0.08688973593\alpha^2 + 20.0004177391150\alpha w^2 + 0.08688973593\alpha^2 w^2 \\ & + 0.00004294498237w \end{aligned} \right) \\
 & + \frac{1}{24}t^4 \left(\begin{aligned} & -0.000006312448556w - 0.002945275534\alpha + 0.003088292280\alpha w + 0.051745978490.\alpha^2 w \\ & - 0.0001397844441\alpha w^2 - 0.02385603518\alpha^2 w^3 - 0.000003232298178w^3\alpha - 0.001344636041w^3\alpha^2 \\ & - 0.5593685934\alpha^3 w - 0.1864561978\alpha^3 w^3 + 0.55993685934\alpha^3 w^2 - 0.02654530726\alpha^2 \\ & - 1.9903988158 \times 10^{-7} w^2 + 0.1864561978\alpha^3 - 2.589982613 \times 10^{-9} w^3 + 0.01594865528 \end{aligned} \right) \\
 R(t) = & 115 + 30.57089998t - 1.257392747t^2 - \frac{1}{6}t^3 \left(\begin{aligned} & 0.003102306530\alpha w - 0.003102306530\alpha + \\ & 0.000007457467620w - 0.2000412843 \end{aligned} \right) \\
 & - \frac{1}{24}t^4 \left(\begin{aligned} & 0.01595932060 + 0.001263809101.\alpha w - 0.01331444442\alpha^2 w - 0.001295814977\alpha \\ & + 3.846860097 \times 10^{-8} w^2 + 0.006657222212\alpha^2 + 0.00003200587600\alpha w^2 + 0.0066 \\ & 57222212\alpha^2 w^2 + 0.000003265518413w \end{aligned} \right)
 \end{aligned}$$

4.1. Numerical Simulation

Here we examine the influence of high risk quarantine w and multiple COVID 19 exposure α on the interval $[0,1)$ to analyze their influence in Control and Spread of COVID-19 respectively. We assess the model's validity by numerically projecting the impact of the induced parameters on the dynamics of transmission of each classes at an increasing time using the baseline parameters in Table 2.

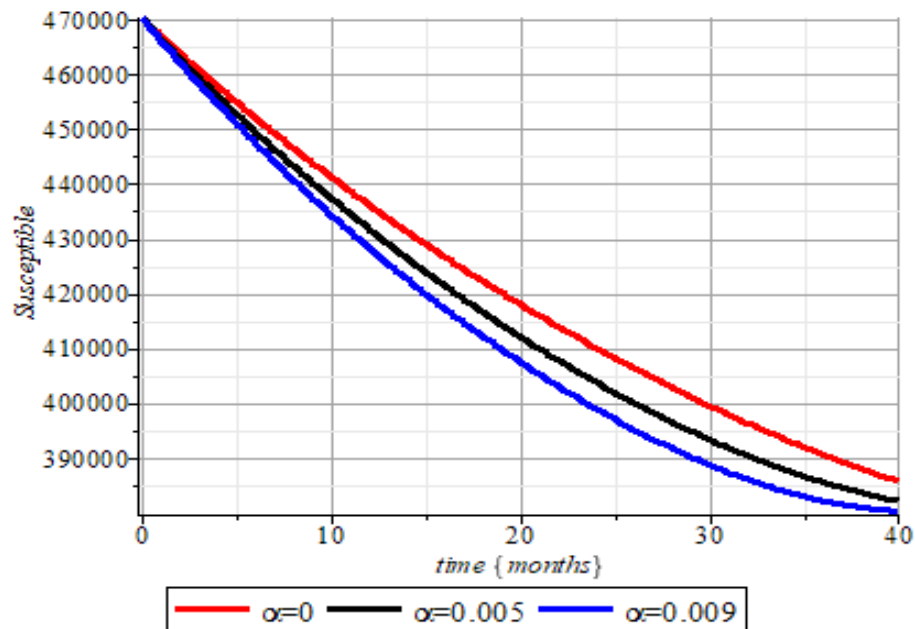


Figure 1: Effect of COVID-19 multiple exposure on susceptible population.

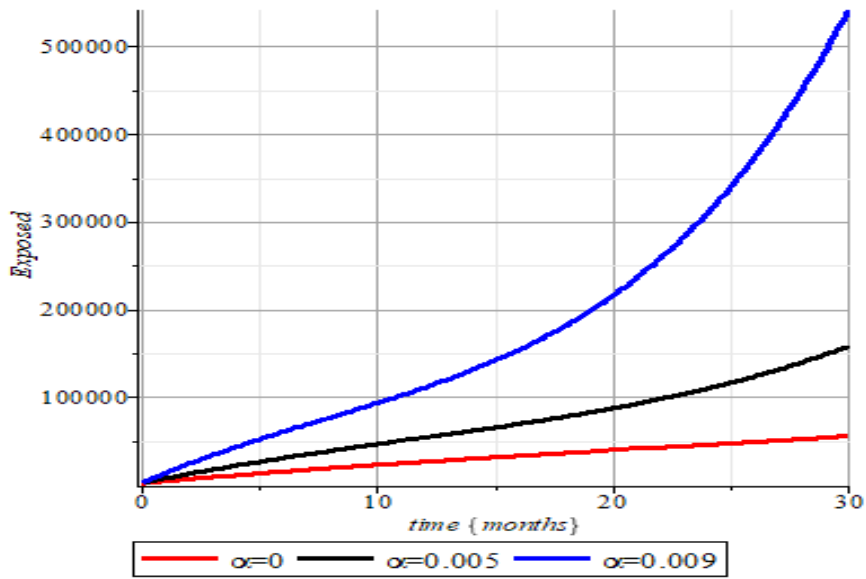


Figure 2: Effect of COVID-19 multiple exposure on Exposed population.

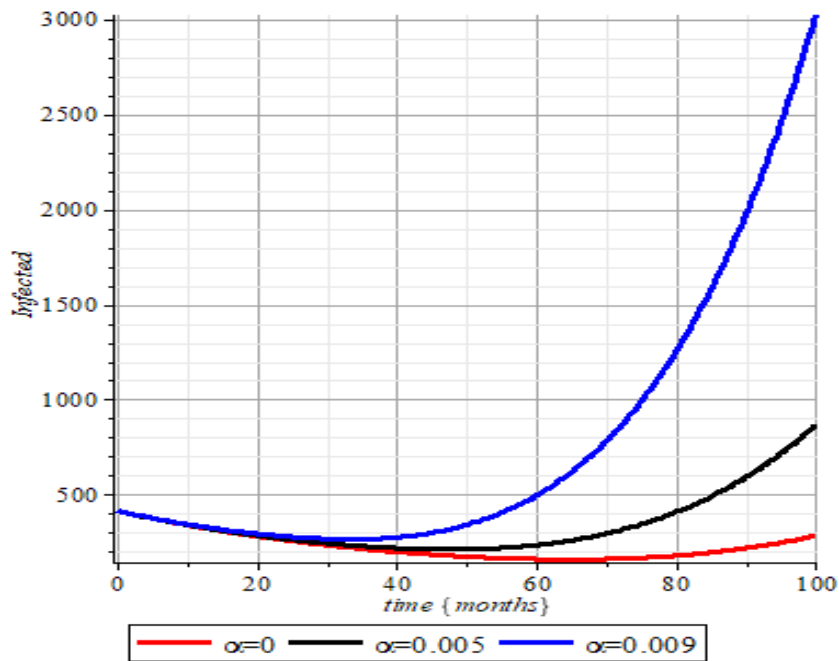


Figure 3: Effect of COVID-19 multiple exposure on Infected population.

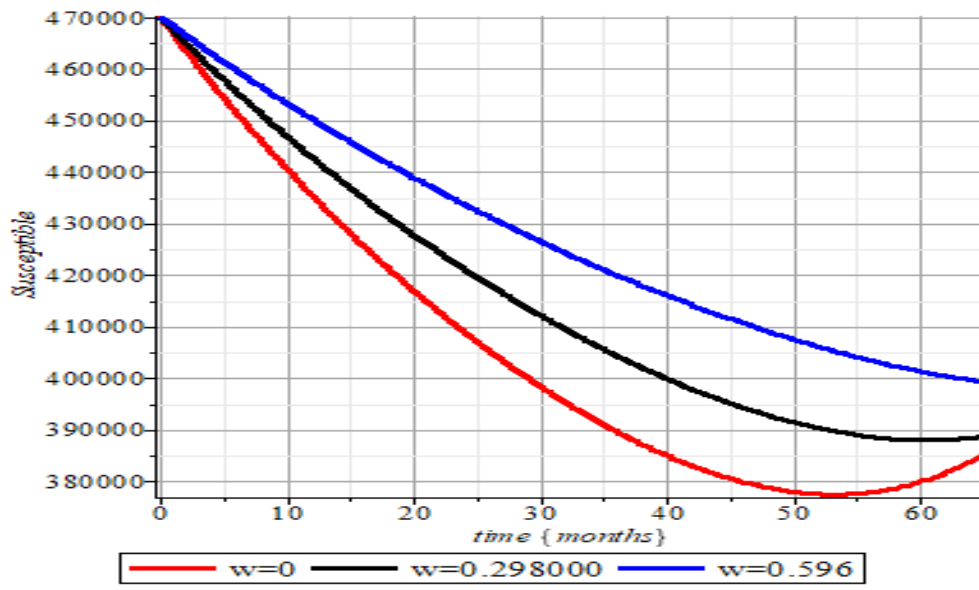


Figure 4: Effect of High risk quarantine on susceptible population.

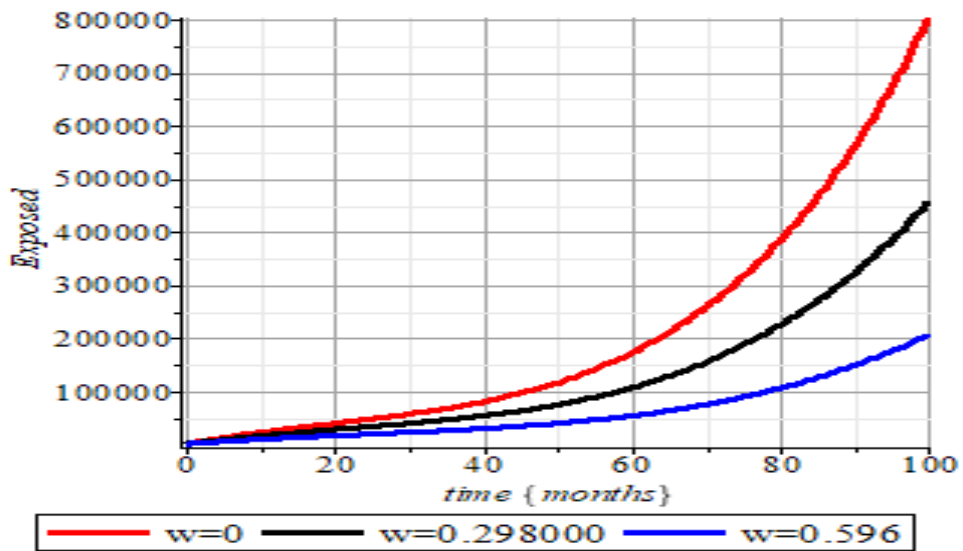


Figure 5: Effect of High-risk quarantine on Exposed population

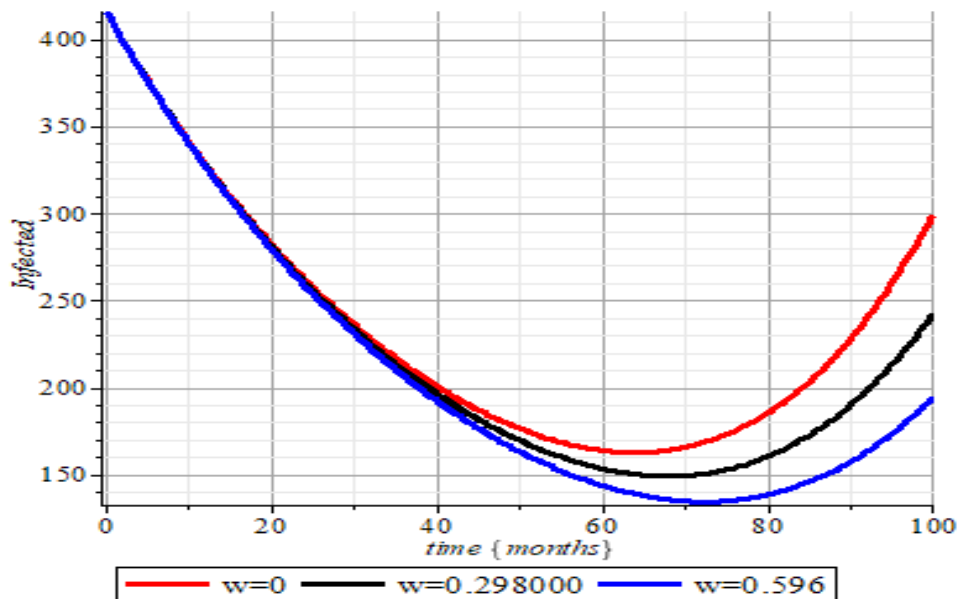


Figure 6: Effect of High risk quarantine on Infected population.

5. Discussion

The figures presented in this section reveal critical insights into the dynamics of COVID-19 transmission and the effectiveness of high-risk quarantine and multiple exposures in controlling its spread. Figure 1 depicts the relationship between the coefficient of multiple exposure and the number of susceptible individuals. As the coefficient of multiple exposures increases, the number of susceptible individuals decreases. This trend can be attributed to the fact that individuals exposed to the virus multiple times are more likely to become infected, transitioning into the exposed or infected populations. Consequently, the susceptible population is reduced. Notably, the graph shows that the rate of decrease in the susceptible population is more pronounced for higher values of the coefficient of multiple exposure. This indicates that multiple exposures have a more substantial impact on reducing the number of susceptible individuals when the exposure rate is higher. In Figure 2, we explore the effect of multiple COVID-19 exposures on the exposed population. As expected, an increase in the coefficient of multiple exposure leads to a rise in the number of exposed individuals. Those who experience repeated exposure to the virus are more susceptible to infection, and as a result, they contribute to the growing number of exposed individuals in the population. Similar to Figure 1, we observe that the rate of increase in the exposed population is more significant for higher values of the coefficient of multiple exposure. This underscores the heightened impact of multiple exposures on increasing the exposed population when the exposure rate is higher. Figure 3 takes a closer look at the impact of multiple COVID-19 exposures on the infected population. As the coefficient of multiple exposure rises, the number of infected individuals also increases. This is understandable, as individuals exposed to the virus multiple times are more susceptible to infection and consequently contribute to the spread of the disease. This finding highlights the importance of mitigating multiple exposures to control the overall infection rate. Shifting our focus to the effect of high-risk quarantine, Figure 4 demonstrates how the number of susceptible individuals is affected by an increase in the high-risk quarantine rate. As the high-risk quarantine rate rises, the number of susceptible individuals decreases. This trend arises from the fact that individuals at high risk of exposure to COVID-19 are more likely to be quarantined, effectively preventing them from contracting the virus and thus reducing the number of susceptible individuals in the population. Figure 5 explores the impact of high-risk quarantine on the exposed population. As the high-risk quarantine rate increases, the number of exposed individuals decreases. This is due to the identification and quarantine of individuals who have been exposed to the virus. By promptly isolating these individuals, we prevent them from becoming part of the infected population and further curtail the spread of the disease. Finally, in Figure 6, we examine the effect of high-risk quarantine on the infected population. As the high-risk quarantine rate

increases, the number of infected individuals decreases. This is because infected individuals are more likely to be identified and isolated through quarantine measures, effectively halting their ability to transmit the virus to others. Consequently, this results in a decline in the infected population. Taken together, these discussion underscore the significance of high-risk quarantine and the impact of multiple exposures on controlling the spread of COVID-19. Implementing measures to identify and quarantine individuals at high risk of exposure or those who have been exposed to the virus can lead to a reduction in the number of susceptible, exposed, and infected individuals in the population, thereby slowing down the transmission dynamics of the disease.

6. Conclusions

To achieve full elimination of COVID-19 outbreaks, we conducted a study examining the effect of High-risk immunity on a COVID-19 positive system with repeated exposure of susceptible individuals. Our research objective was accomplished as the numerical simulation results clearly illustrated the transmission of COVID-19 under High-risk immunity conditions with multiple exposures. To eliminate the virus, we advise widespread immunization of vulnerable populations. The efficacy of governmental control measures to mitigate transmission can only be realized through public cooperation in adhering to preventative measures such as curfew, self-isolation, and proper utilization of face masks. The complete elimination of COVID-19 requires collective efforts from all individuals to strictly abide by these preventive measures. Our study highlighted the various responses of a vulnerable population to High-risk immunity with repeated exposure. Future studies could consider combining the examination of proportional vaccination and High-risk immunity. Furthermore, utilizing fractional order analysis in the existing mathematical model through the implementation of fractional operators such as Caputo [25], Caputo-Fabrizio [26], or Antangana-Baleanu [27] could provide a more in-depth evaluation of the disease's dynamics using actual data.

Acknowledgements

The authors acknowledge the efforts of all academic staffs of the Department of Mathematical Sciences, of Osun State University.

Declaration of Competing Interest

The authors declare no conflict of interest.

Authorship Contribution Statement

Mutairu Kolawole: Data preparation, analysis, reviewing, supervision

Morufu Olayiwola: Conceptualization, methodology, analysis, supervision

Adedapo Alaje: Writing, computations, simulation, analysis and discussion

Kazeem Abidoje: Typesetting, qualitative analysis, discussion

References

- [1] R.C. Del, and P.N. Malani, "Covid-19 New insights on a rapidly changing epidemic," *JAMA*, vol. 323, no. 14, pp. 1339-1340, 2020.
- [2] WHO (World Health Organization) "2020 Emergencies, preparedness, response. Pneumonia of unknown origin-China, Disease Outbreak News," <https://www.who.int/csr/don/05-january-2020-pneumonia-of-unknowncause-china/en/> (accessed 5 March 2020).

- [3] C. C. Lai, T. P. Shih, W. C. Ko, H. J. Tang, and P. R. Hsueh, "Severe acute respiratory syndrome coronavirus 2 (SARS-CoV-2) and coronavirus disease-2019 (COVID-19): The epidemic and the challenges," *International journal of antimicrobial agents*, vol. 55, no. 3, pp. 105924, 2020.
- [4] Q. Li, X. Guan, P. Wu, X. Wang, L. Zhou, Y. Tong, R. Ren, K. S. Leung, E.H. Lau, J.Y. Wong, and X. Xing, "Early transmission dynamics in Wuhan China of novel coronavirus infected pneumonia," *The New England journal of medicine*, vol. 382, no. 13, pp. 1199-1207, 2020.
- [5] F. Bozkurt, A. Yousef, T. Abdeljawad, A. Kalini, Q. Al Mdallal, "A fractional order model of COVID-19 considering the fear effect of the media and social networks on the community," *Chaos, Solitons and Fractals*, vol. 152, pp. 111403, 2021.
- [6] R. U. Din, E. A. Algehyne, "Mathematical analysis of COVID-19 by using SIR model with convex incidence rate," *Result in Physics*, vol. 23, pp. 103970, 2021.
- [7] R. U. Din, K. Shah, I. Ahmad, T. Abdeljawad, "Study of transmission dynamics of novel COVID-19 by using mathematical model," *Advances in Difference Equations*, vol. 2020, pp. 323, 2020.
- [8] O. J. Peter, S. Qureshi, A. Yusuf, M. Al-Shomrani, and A. A. Idowu, "A new mathematical model of COVID-19 using real data from Pakistan," *Results in Physics*, vol. 24, pp. 104098, 2021.
- [9] L. Wang, F. Xinjie, S. Yongzheng, and L. Maoxing, "Dynamical Analysis of a mathematical model of COVID-19 Spreading on Networks," *Frontiers in Physics*, vol. 8, 2021.
- [10] R. U. Din, and E. A. Algehyne, "Mathematical analysis of COVID-19 by using SIR model with convex incidence rate," *Result in Physics*, vol. 23, pp. 103970, 2021.
- [11] A. Khan, R. Zarin, G. Hussain, N.A. Ahmad, M. H. Mohd, and A. Yusuf, "Stability analysis and optimal control of Covid-19 with convex incidence rate in Khyber Pakhtunkhawa (Pakistan)," *Results Physics*, vol. 20, pp. 103703, 2021.
- [12] O. J. Peter, S. Qureshi, S. Yusuf, M. Shomrani, and A. A. Idowu, "A new mathematical model of COVID-19 using real data from Pakistan," *Results in Physics*, vol. 24, pp. 104098, 2021.
- [13] A. I. Alaje, M. O. Olayiwola, M. O. Ogunniran, J. A. Adedeji, and K. A. Adedokun, "Approximate analytical methods for the solution of fractional order integro-differential equations," *Nigerian Journal of Mathematics and Applications*, vol. 31, pp. 175-190, 2021.
- [14] S. Triambak, D. P. Mahapatra, N. Mallick, and R. Sahoo, "A new logistic growth model applied to COVID-19 fatality data," *Epidemics*, vol. 37, pp. 100515, 2021.
- [15] A. Babaei, H. Jafari, S. Banihashemi, and M. Ahmadi, "Mathematical analysis of a stochastic model for spread of Coronavirus," *Chaos Solitons Fractals*, vol. 145, pp. 110788.
- [16] A.O. Yunus, M. O. Olayiwola, K. A. Adedokun, J. A. Adedeji, and A. I. Alaje, "Mathematical analysis of fractional-order Caputo's derivative of coronavirus disease model via Laplace Adomian decomposition method," *Beni-Suef Univ J Basic Appl Sci*, vol. 11, no. 144, 2022.
- [17] C. Xu, Z. Liu, Y. Pang, and A. Akgül, "Stochastic analysis of a COVID-19 model with effects of vaccination and different transition rates: Real data approach," *Chaos, Solitons and Fractals*, vol. 170, pp. 113395, 2023.
- [18] J. H. He, "Homotopy perturbation technique," *Comput. Methods. Appl. Mech. Eng.* vol. 178, pp. 257-262. 1999.
- [19] S. Balamuralitharan, and S. Geethamalini, "Solutions of epidemic of EIAV infection by HPM," *Journal of Physics. Conf.Series*, vol. 1000, pp. 012023, 2018.
- [20] M. K. Kolawole, A. I. Alaje, M. O. Ogunniran, and K. R. Tijani, "Simulating the effect of disease transmission coefficient on a disease induced death seirs epidemic model using the homotopy perturbation method," *Journal of Applied Computer Science & Mathematics*, vol. 16, no. 33, 2022.
- [21] M. O. Olayiwola, A. W. Gbolagade, and F. O. Akinpelu, "An efficient algorithm for solving the nonlinear PDE," *International Journal of Scientific and Engineering Research*, vol. 2, no. 10, pp. 1-10, 2011.
- [22] M. O. Ogunniran, Y. Haruna, and R. B. Adeniyi, and M. O. Olayiwola, "Optimized three-step hybrid block method for stiff problems in ordinary differential equation," *Çankaya University Journal of Humanities and Social Sciences*, vol. 17, pp. 80-95, 2020.
- [23] M. O. Olayiwola, F. O. Akinpelu, and A. W. Gbolagade, "Modified variational iteration method for the solution of a class of differential equations," *American Journal of Computational and Applied Mathematics*, vol. 2, no. 5, pp. 228-231, 2012.

- [24] Ikeja City Population [Online] Accessed (26-12-2022).
https://citypopulation.de/en/nigeria/admin/lagos/NGA025011__ikeja
- [25] M. Caputo, "Elasticita e Dissipazione," Zanichelli, Bologna 14, 1969.
- [26] M. Caputo, and M. Fabrizio, "A new definition of fractional derivative without singular kernel," *Prog. Fract. Difer. Appl.* vol. 1, no. 2, pp. 73–85, 2016.
- [27] A. Atangana, and D. Baleanu, "New fractional derivatives with non-local and nonsingular kernel theory and application to heat transfer model," *Therm. Sci.* vol. 20, pp. 763–769, 2016.